Liquid Crystals
Publication details, including instructions for authors and subscription information:
http://www.informaworld.com/smpp/title~content=t713926090

Synthesis and thermotropic liquid-crystalline properties of N-alkylpyridinium bromides substituted with a terphenylene moiety

R. G. Santos-Martell[a]; A. Ceniceros-Olguín[a]; L. Larios-López[a]; R. J. Rodríguez-González[a]; D. Navarro-Rodríguez[a]; B. Donnio[b]; D. Guillon[b]
[a] Centro de Investigación en Química Aplicada (CIQA), Saltillo, Coahuila, Mexico [b] Institut de Physique et Chimie des Matériaux de Strasbourg (IPCMS), UMR 7504 (CNRS-Université Louis Pasteur), Strasbourg Cedex, France

To cite this Article Santos-Martell, R. G. , Ceniceros-Olguín, A. , Larios-López, L. , Rodríguez-González, R. J. , Navarro-Rodríguez, D. , Donnio, B. and Guillon, D.(2009) 'Synthesis and thermotropic liquid-crystalline properties of N-alkylpyridinium bromides substituted with a terphenylene moiety', Liquid Crystals, 36: 8, 787 — 797
To link to this Article: DOI: 10.1080/02678290903060618
URL: http://dx.doi.org/10.1080/02678290903060618

Liquid Crystals,
Vol. 36, No. 8, August 2009, 787–797

Taylor & Francis
Taylor & Francis Group

Synthesis and thermotropic liquid-crystalline properties of N-alkylpyridinium bromides substituted with a terphenylene moiety

R.G. Santos-Martell[a], A. Ceniceros-Olguín[a], L. Larios-López[a], R.J. Rodríguez-González[a], D. Navarro-Rodríguez[a]*, B. Donnio[b] and D. Guillon[b]

[a]*Centro de Investigación en Química Aplicada (CIQA), Blvd. Enrique Reyna 140, CP 25253, Saltillo, Coahuila, Mexico;* [b]*Institut de Physique et Chimie des Matériaux de Strasbourg (IPCMS), UMR 7504 (CNRS-Université Louis Pasteur), 23 rue de Loess, 67037 Strasbourg Cedex, France*

(Received 19 December 2008; final form 21 May 2009)

Molecules containing a terphenylene core, two alkyl chains and a pyridinium ring associated with its bromine counterion were synthesised and their liquid crystalline properties were studied by differential scanning calorimetry, polarising optical microscopy and X-ray diffraction. The results were compared with those of chemical intermediates, which also develop a liquid crystalline behaviour. Both intermediates and pyridinium salts showed a rich polymorphism at temperatures ranging from around 100 to 200°C and 115 to 220°C, respectively. X-ray results indicate that both intermediates and pyridinium salts develop tilted smectic mesophases with molecules stacked in single and double layers, respectively. The tilt angle of some of these compounds decreases so markedly upon cooling that molecules attain almost an orthogonal position. The stacking of molecules in the smectic layers was explained in terms of the mutual repulsion interactions between the terphenylene core, the alkyl chains and the ionic species (the pyridinium ring associated with its counterion) and it was proposed that the π–π interactions between the long aromatic cores counterbalance the strong forces between the ionic species, leading to a full segregation of these molecular parts in periodic sublayers. A molecular arrangement model is proposed for these salts.

Keywords: terphenylene; pyridinium salts; mesomorphic; smectic

1. Introduction

In recent years there has been an increasing interest in the synthesis and study of π-conjugated molecules developing both liquid crystalline (LC) and light emission (LE) properties (*1*, *2*). The combination of these two characteristics in just one molecule is of technological interest, because thin films with molecular emitters, possessing a preferential orientation, can be readily obtained from LC molecules (*3–6*). Organic light-emitting diodes (OLEDs), built with films containing aligned luminescent molecules, produce a linearly polarised LE that could be used as a backlight in flat panel displays and other applications. In this regard much research work has been done on π-conjugated polymers developing both LC and LE properties (*7–9*); however, it was observed that small π-conjugated molecules with few units (oligomers) show a richer polymorphism at lower temperatures and similar optical emission characteristics with respect to their polymer counterparts (*10*). In addition, conjugated oligomers with a determined chemical structure (*11*) and different lengths (*12*) can easily be synthesised through well-known chemical procedures. In a recent paper we have reported a series of alkyloxy modified oligophenylenes (3, 5 and 7 phenylene units) developing nematic and smectic C (SmC) mesophases and showing a LE in the blue region ($\lambda \sim$ 400 nm) (*13*). Among these oligomers, those bearing a terphenylene unit showed the richest polymorphism at lower temperatures. These alkyloxy-substituted terphenylenes were functionalised at one chain end with bromine to obtain intermediates (*14*), which were further used to quaternise a pyridine cycle producing novel amphiphiles also showing LE and LC properties. Such amphiphiles combine in the same molecule three parts of different nature: a long aromatic core (terphenylene), two alkyl chains and a pyridinium ring associated with its counterion. From this molecular composition we would expect either a full segregation of molecular parts in microdomains, periodically arranged in space, or a partial segregation resulting from the strong interaction between the ionic parts that overbalance the interaction forces of the other moieties, as was observed in analogous molecules bearing a biphenyl mesogenic group (*15*). The number of ionic liquid crystals is still limited, and the field has the potential for a strong expansion.

*Corresponding author. Email: damaso@ciqa.mx

ISSN 0267-8292 print/ISSN 1366-5855 online

DOI: 10.1080/02678290903060618
http://www.informaworld.com

The introduction of different features in molecular structures is a demanding and challenging task and the resulting mesophases could be interesting for multiple applications, as stated by Binnemans in his excellent review on this concern (*16*). In the present work, the synthesis and the thermotropic LC properties of new N-alkylpyridinium bromides substituted with a terphenylene moiety are described and discussed.

2. Experimental

2.1 Characterisation

^{1}H NMR spectra were recorded with a 300 MHz Jeol spectrometer using tetrahydrofuran (THF)-d_8 or $CDCl_3$ as solvents. Differential scanning calorimetry (DSC) traces were obtained from a MDSC 2920 from TA Instruments at heating and cooling rates of 5°C min^{-1}. The thermal stability was determined by using a thermal analyser (TGA Q500) from TA Instruments. Optical textures of mesophases were registered upon heating and cooling in an Olympus BH-2 polarising optical microscope coupled with a Mettler FP82HT hot stage. X-ray diffraction (XRD) patterns were recorded with an INEL CPS120 diffractometer ($K_{\alpha 1}$, cooper radiation and home-made electrical oven).

2.2 Materials

4-Bromophenol, 4′-bromo-4-hydroxybiphenyl, 1-bromotetradecane, 1-bromohexadecane, 1,8-dibromooctane, 1, 12–dibromododecane, bromine, butyllithium 1.6M in hexanes, triisopropylborate, tetrakis(triphenylphosphine)palladium(0), sodium carbonate, hydrochloric acid (37%), pyridine, dimethylformamide (DMF), THF, dichloromethane, methanol, ether, chloroform-*d* and THF-*d* were purchased from Aldrich Co. or J. T. Baker. All these materials were used as received, except for THF, which was distilled from a sodium/benzophenone complex before use, and pyridine, which was distilled from a pyridine/KOH mixture under reduced pressure at 65°C.

2.3 Synthesis

The intermediates and final molecules were synthesised and purified by using the reported procedures (*13*, *15*). The chemical reactions involved (Figure 1) are as follows.

i. A Williamson reaction (*17*) to introduce the alkyl chain and the bromine end-functionalised alkyl chain into the 4′-bromo-4-hydroxybiphenyl and the 4-bromophenol, respectively. In both reactions DMF and 10% molar excess of NaOH were used.
ii. A boronation reaction to obtain an aryl boronic acid from the 4′-bromo-4-alkyloxybiphenyl and triisopropylborate (*18*). This reaction was carried out in two steps: In the first step the 4′-bromo-4-alkyloxybiphenyl was dissolved in THF at –40°C and then butyllithium (1.6 M in hexanes) was added dropwise while the solution was maintained under vigorous stirring. In the second step the *in situ*-formed lithium-aryl complex was reacted with triisopropylborate to obtain the aryl boronic acid.
iii. A Suzuki coupling reaction (*19*) between the arylboronic acid and the 4-(ω-bromoalkyloxy)bromophenyl catalysed with a Pd(0)-complex to obtain the 4-(ω-bromoalkyloxy)-4″alkyloxyterphenylenes (T*n-m* compounds). The reaction was carried out in freshly distilled THF in the presence of Na_2CO_3.
iv. The quaternisation reaction was carried out as follows: in a one neck round-bottom flask, equipped with magnetic stirring and an inert gas inlet (argon), 50 mL of freshly distilled pyridine and 0.615 mmol of the corresponding T*n-m* compound were introduced. The solution was degassed, stirred and heated up to 90°C. The reaction was allowed to proceed for 14 hours and then it was cooled down to room temperature. The resulting pyridinium salt (P*n-m* compound) was recuperated by precipitation and filtration. The salt was finally washed thoroughly with ether. In all reactions a white fine powder was obtained with yields higher than 85%.

For the sake of brevity, intermediates and pyridinium salts were labelled as T*n-m* and P*n-m*, respectively, where '*n*' and '*m*' indicate the length of the terminal alkyl chain and the spacer, respectively.

3. Results and discussion

3.1 Synthesis

Pyridinium salts were obtained through the synthesis route described in the previous section (reactions *i* to *iv* in Figure 1). This route is quite convenient because boronic acids are fairly stable and readily react with arylbromides under mild conditions (*20*). In addition, boronic acids can be stored for a long time and used when required. On the other hand, the quaternisation of the pyridine cycle can be carried out in different solvents of

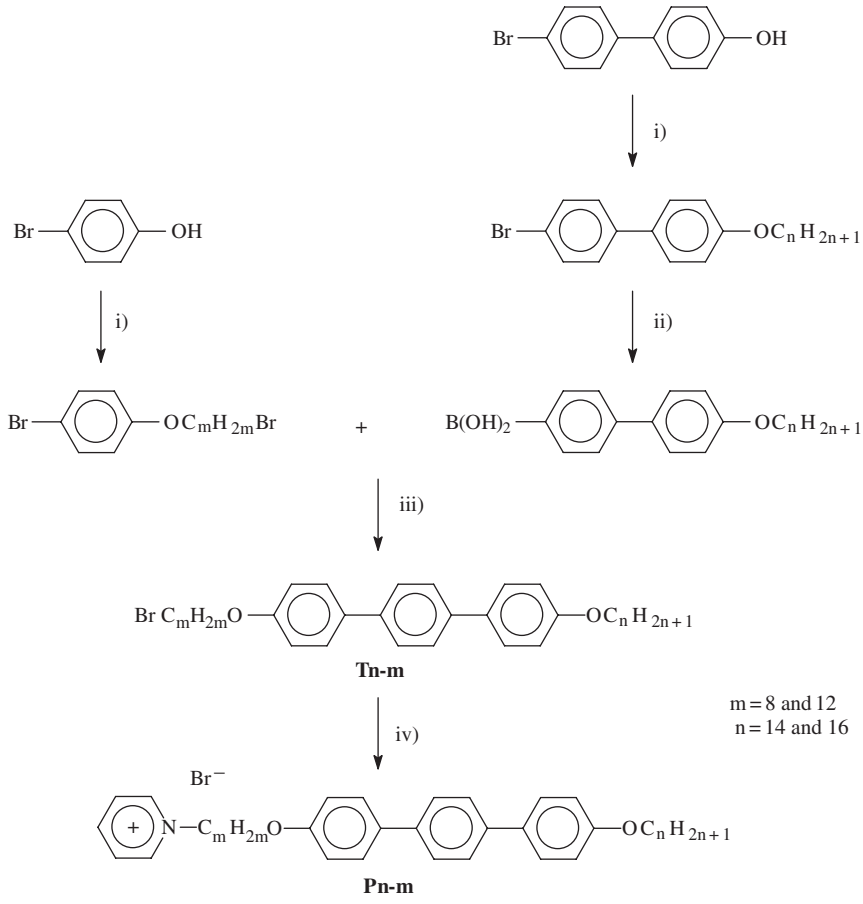

Figure 1. Synthesis route for the preparation of pyridinium salts containing a terphenylene moiety.

high dielectric constants, such as DMF and methanol, among others; however, pyridine by itself is the most suitable solvent/reactive because its dielectric constant is relatively high (ε = 12.3) and also because it dissolves the T*n-m* compounds quite well and the reaction takes place without side reactions (*15*). All compounds were analysed by ^{1}H NMR spectroscopy; however, only two spectra (one of each series) are shown to demonstrate the structure and purity of compounds.

Figure 2 shows the ^{1}H NMR spectrum of compound **T16-12**. Chemical shifts at δ = 6.9 and 7.55 ppm correspond to the aromatic protons. Those at δ = 3.4 and 4 ppm were assigned to the protons of the methylene groups linked to the bromine and oxygen atoms, respectively. Signals at 1.2–2.0 ppm correspond to the protons of the internal methylenes of alkyl chains, while that at 0.9 ppm corresponds to those of the methyl group.

Figure 3 shows the ^{1}H NMR spectrum of compound **P16-12**. Most signals are similar to those of compound **T16-12**, except for those observed at 8.0–9.5 ppm and 5.1 ppm, which correspond to the protons of the pyridinium ring and to the methylene group linked to the nitrogen atom, respectively (*21*). The protons of the methylene group in the β position with respect to the nitrogen atom can be also distinguished at 2.1 ppm.

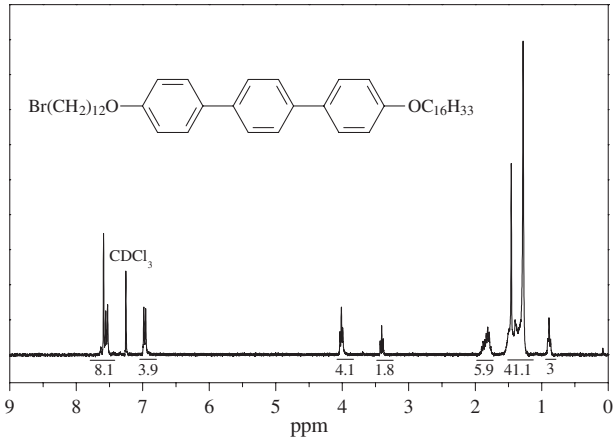

Figure 2. ^{1}H NMR spectrum of **T16-12**. Solvent $CDCl_3$.

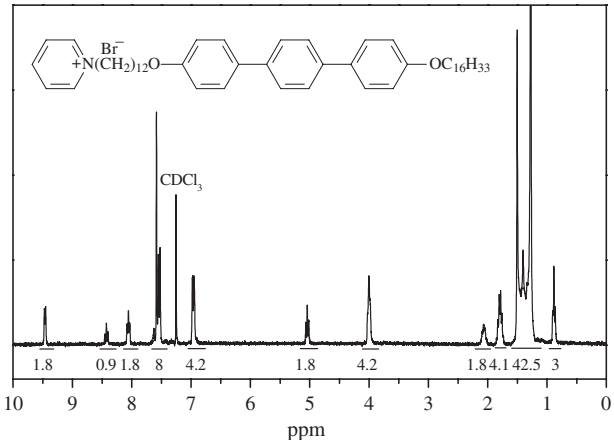

Figure 3. ^{1}H NMR spectrum of **P16-12**. Solvent $CDCl_3$.

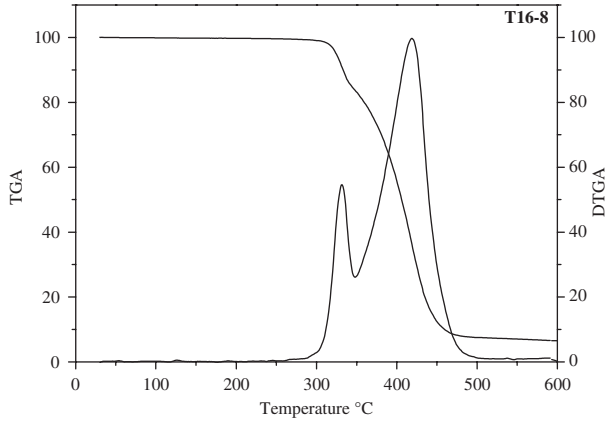

Figure 4. TGA thermogram of **T16-8**.

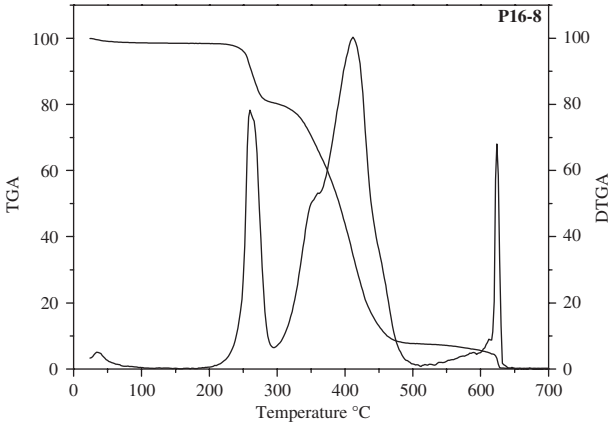

Figure 5. TGA thermogram of **P16-8**.

All of these signals indicate that the quaternisation reaction has occurred as expected.

3.2 Thermal stability

Thermogravimetric analysis (TGA) data shown in Table 1 indicate that the T*n-m* and P*n-m* compounds are thermally stable up to 316–345°C and 241–255°C, respectively. This significant difference in thermal stability arises from the CH_2–N^+ bond in the P*n-m* compounds, which is poorly resistant to heating (*22*). The initial decomposition temperature T_d for both T*n-m* and P*n-m* seems to be more dependent on the terminal chain length than on the spacer length (Table 1); that is, intermediates and pyridinium salts containing a terminal chain C14 decompose at higher temperatures than those bearing a terminal chain C16. TGA traces of **T16-8** (Figure 4) and **P16-8** (Figure 5) were selected as representative examples of the T*n-m* and P*n-m* series, respectively. It should be pointed out that pyridinium molecules develop multiple thermal transitions (observed by DSC and polarised optical microscopy (POM)), showing signs of degradation below the clearing point.

Table 1. Initial temperature decomposition (T_d) for the T*n-m* and P*n-m* series.

T*n-m*	T_d/°C	P*n-m*	T_d/°C
T14-8	345	**P14-8**	255
T14-12	345	**P14-12**	255
T16-8	316	**P16-8**	247
T16-12	333	**P16-12**	241

3.3 Thermotropic behaviour

The LC properties of both T*n-m* and P*n-m* compounds were initially studied by DSC and optical microscopy. At this point, it is opportune to mention that the transition temperatures and enthalpy changes of the T*n-m* series were presented and discussed in a previous communication (*14*). In the present document, additional data on these compounds are presented in order to compare with the thermotropic behaviour of the synthesised pyridinium salts.

All T*n-m* and P*n-m* compounds exhibited multiple thermal transitions in both heating and cooling scans, as shown in Figure 6 for compound **T14-8** and in Figures 7 and 8 for compounds **P14-8** and **P14-12**, respectively. As was already mentioned, pyridinium salts remain in a mesomorphic state even at the decomposition temperature. In fact, it was difficult to determine the clearing point due to such decomposition.

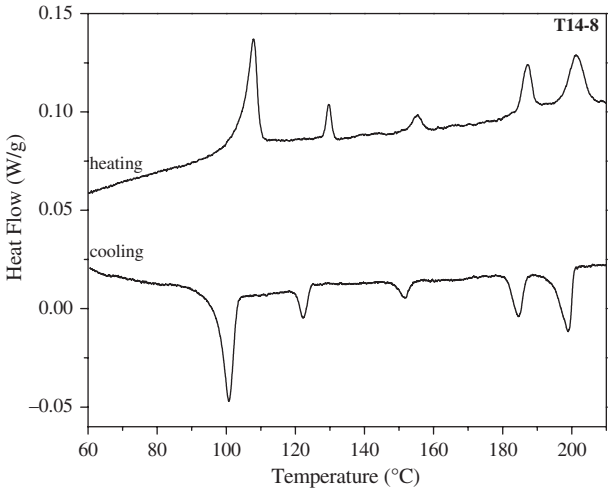

Figure 6. Heating and cooling DSC traces at 5°C min^{-1} for compound **T14-8**.

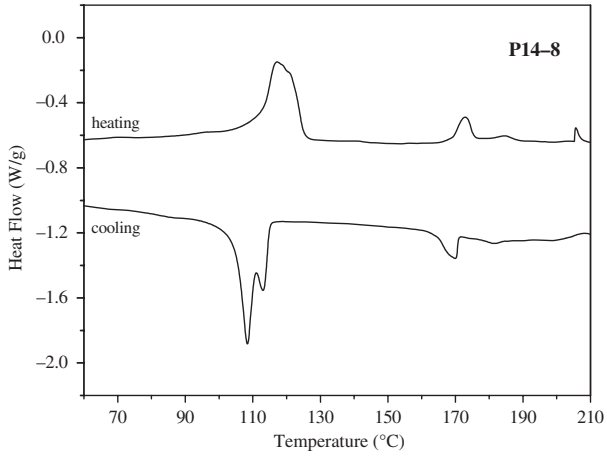

Figure 7. Heating and cooling DSC traces at 5°C min^{-1} for compound **P14-8**.

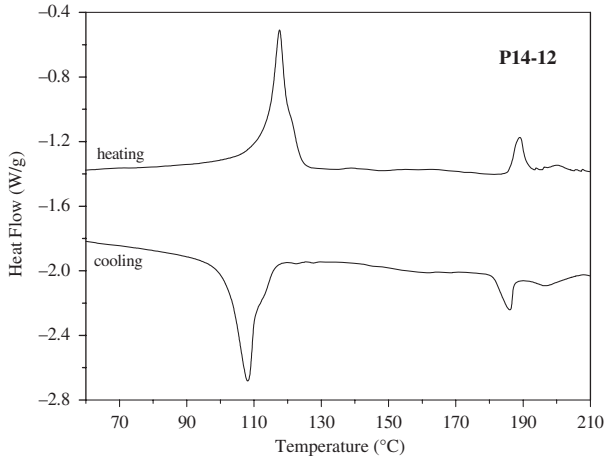

Figure 8. Heating and cooling DSC traces at 5°C min^{-1} for compound **P14-12**.

On the other hand, the optical textures for the T*n-m* compounds were clearer than those observed for the pyridinium salts. For the T*n-m* compounds, typical focal-conic (Figure 9) and *Schlieren* (Figure 10) textures were observed. In contrast, for the P*n-m* compounds the textures were non-specific (Figure 11), except for those obtained at high temperature for the compound **P14-12** (Figure 12) that were identified as *Schlieren* and focal-conic textures.

3.4 Structure of mesophases

XRD analysis was used to ascertain the nature of the mesophases observed by DSC and optical microscopy

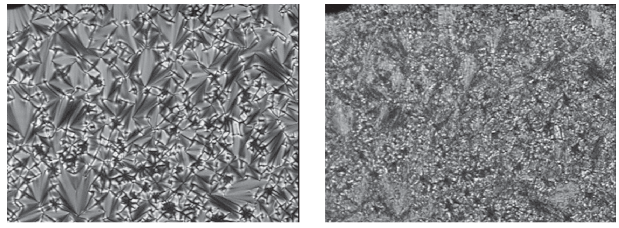

180°C 150°C

Figure 9. Optical textures obtained for compound **T14-8** at two different temperatures.

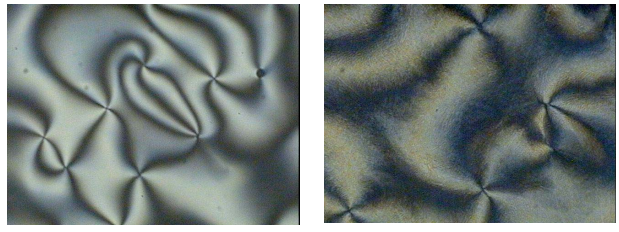

160°C 140°C

Figure 10. Optical textures obtained for compound **T14-12** at two different temperatures.

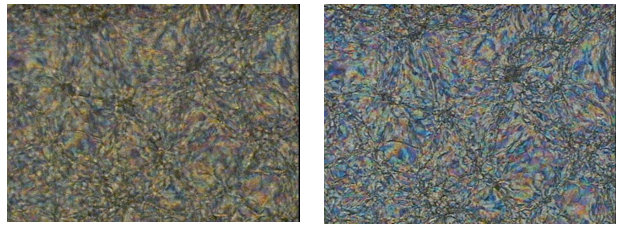

180°C 150°C

Figure 11. Optical textures obtained for compound **P14-8** at two different temperatures.

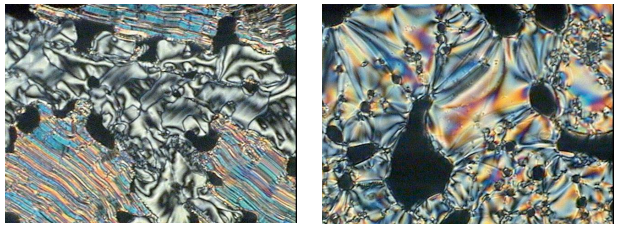

200°C 200°C

Figure 12. Optical textures obtained for compound **P14-12** at 200°C. First (left) and second (right) heating.

and also to determine their structural parameters. For intermediates, only the XRD spectra of the **T14-8** sample (Figure 13), recorded at different temperatures, were selected to be discussed as representative examples.

X-ray patterns of the T*n-m* series were characterised by the presence of one Bragg sharp reflection at low angles (001), which denotes the smectic nature of the liquid-crystalline phases. The stacking period of the smectic layers (d_{001}), measured experimentally, was compared with the length of the molecule in its most extended conformation (L), calculated by using molecular modelling software from Chem Sketch ACD/Labs (Table 2). According to the d_{001}/L ratio, all smectic phases of the T*n-m* compounds are single layered. For both **T14-12** and **T16-12**, the calculated d_{001}/L ratio (<1) indicates that molecules are tilted with respect to the normal of the smectic plane at an angle θ ($\cos\theta = d_{001}/L$) higher than 30°. On the other hand, the arrangement of molecules within the smectic layers was determined from the signal appearing in the wide-angle region of the XRD pattern. At 180°C, the pattern showed a broad peak, indicating a liquid-like ordering of molecules within the smectic layers that would correspond to a SmC phase. On

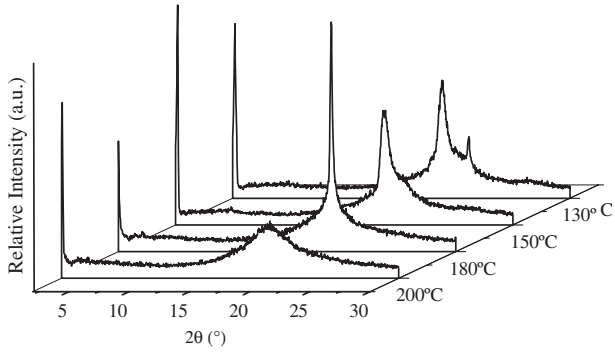

Figure 13. XRD patterns of compound **T14-8** at four different temperatures (on cooling).

Table 2. Structural parameters calculated from the XRD spectra obtained at different temperatures for the T*n-m* series.

T*n-m*	*T*/°C	*L*/Å	d_{001}/Å	Tilt angle/°
T14-8	200	46.1	43.7	18.6
	180		45.1	12.0
	150		41.3	26.4
T14-12	180	51.1	40.3	37.9
	160		40.7	37.2
	150		39.1	40.1
T16-8	200	48.6	46.5	17.0
	180		50.3	0.0
	160		45.9	19.2
T16-12	180	53.6	43.9	35.0
	160		46.4	30.0
	140		44.2	34.4

cooling down to 160°C, such a broad signal becomes sharper, indicating a hexatic-type ordering of molecules within the smectic layers that could be assigned to a smectic F or a smectic I phase. On cooling further, the sharp peak seems to decouple into two signals; one broad dominant signal (~4.5–4.6 Å) and one rather sharp peak (~4 Å), the latter shifted towards higher angles. In some reports of conjugated molecules, such a sharp signal is attributed to the occurrence of π–π type interactions, which appears to be quite common in the molecular packing of long-conjugated aromatic cores (*10*). We have found some works reporting π–π interactions at distances of around 3.8–4 Å, which is similar to those values observed in our molecules. Such reports concern phenylethynylene oligomers (*23*) and conjugated oligoquinolines bearing a conjugated phenylene group (*24*). On the other hand, the calculated d_{001}/L ratio (~1) for compounds **T14-8** and **T16-8** indicates that molecules are rather in an orthogonal position with respect to the smectic plane. At 200°C, the XRD spectrum shows a broad peak in the wide angles region, which is associated with the liquid-like ordering of molecules. Thus, at high temperature (200°C), the mesophase developed by these compounds is rather of the smectic-A type. On cooling down to 180°C, d_{001} shifts to lower angles in such a way that the experimental lamellar distance (d_{001} = 50.3 Å) becomes even a little higher than the corresponding calculated molecular length (48.6 Å), although this difference is not significant enough to consider a molecular stacking different to that of a monolayer-type mesophase. In addition, at 180°C the broad signal becomes sharper, indicating a hexatic-type ordering that could be assigned to a smectic-B type phase. On cooling further, the sharp peak decouples into one broad and one sharp peak, as was observed

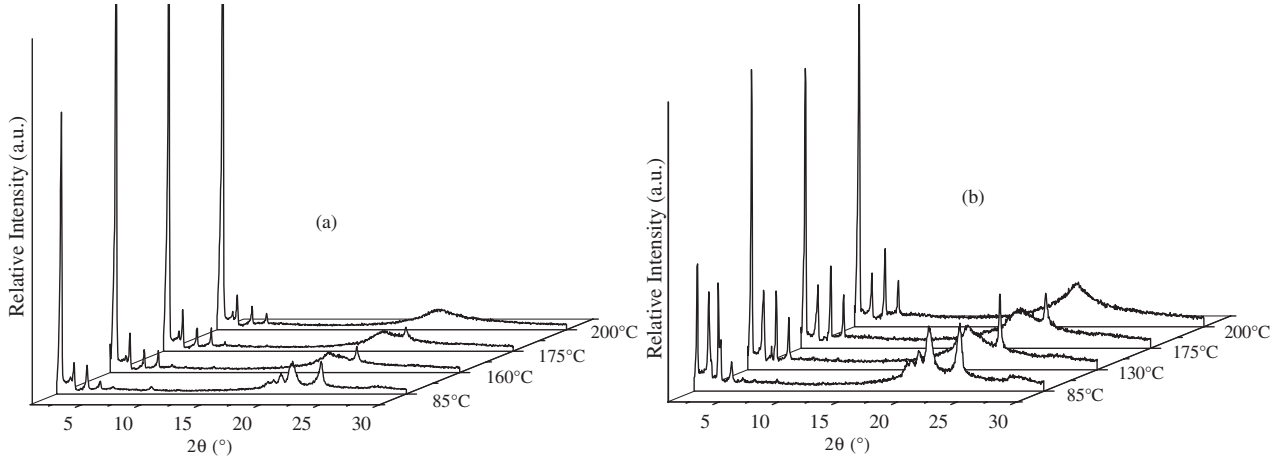

Figure 14. XRD patterns obtained at different temperatures (on cooling) for compounds **P14-8** (a) and **P14-12** (b).

for compounds **T14-12** and **T16-12**. At low temperature all compounds of the T*n-m* series showed multiple sharp Bragg reflections (spectra not shown here), which are characteristic of crystallised samples. The occurrence of orthogonal and tilted mesophases in homologous molecular series has been well documented in the literature (*25*). It appears that tilted mesophases are exhibited at certain terminal alkyl chain length and predominantly in molecules having two terminal flexible groups and possessing some structural symmetry. The occurrence of tilted mesophases in compounds **T14-12** and **T16-12** is certainly associated with these structural characteristics.

XRD patterns (Figures 14 and 15) obtained for the P*n-m* series showed some differences compared to those of intermediates. At low angles, all XRD patterns for the P*n-m* compounds showed one strong and three or more small equidistant Bragg reflections, indicating a well-developed, layered structure of molecules. The experimental stacking period (d_{001}) was also compared with the length of the molecule in its most stretched conformation, calculated by using molecular modelling software. In such modelling the bromine counterion was positioned in front of the pyridinium ring, as sketched in Figure 16. The calculated d_{001}/L ratios (Table 3) indicate that mesophases are double layered with molecules tilted with respect to the normal of the smectic plane. On cooling, the tilt angle decreases from one transition to the other for all P*n-m* compounds, although such decrease was particularly pronounced for compounds **P14-8** and **P14-12**, whose d_{001} value approaches $2L$, meaning that these molecules adopt an almost orthogonal position. A proposed model for

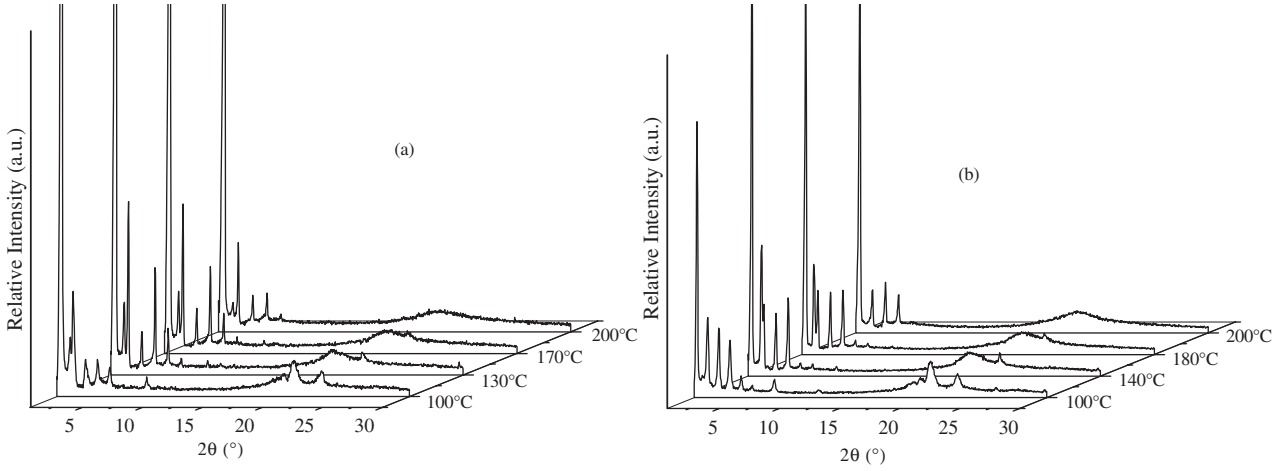

Figure 15. XRD patterns obtained at different temperatures (on cooling) for compounds **P16-8** (a) and **P16-12** (b).

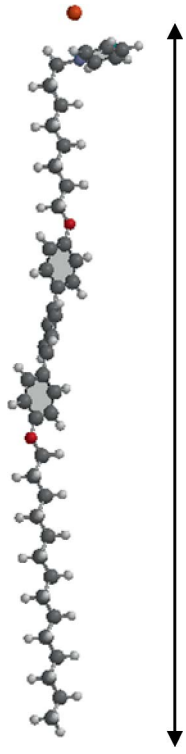

Figure 16. Extended conformation of **P14-8**, modelled by Chem Sketch ACD/Labs.

Table 3. Structural parameters calculated from the XRD spectra obtained at different temperatures for the P*n-m* series.

P*n-m*	*T*/°C	*L*/Å	d_{001}/Å	Tilt angle/°
P14-8	200	43.7	76.9	28.4
	175		79.1	25.1
	160		79.5	24.5
	130		86.1	10
P14-12	200	48.7	85.6	28.5
	175		87.8	25.6
	130		90.5	21.7
	85		95.7	6.7
P16-8	200	46.1	79.3	30.6
	170		82.9	26.0
	130		84.7	23.3
	100		87.4	18.6
P16-12	200	51.0	88.1	30.4
	180		91.0	26.9
	140		92.6	24.8
	100		98.8	14.3

this molecular arrangement is presented in Figure 17. On the other hand, it can be noticed in the patterns that, at high temperature, all P*n-m* compounds developed a broad signal in the wide angles region typical of a liquid-like ordering that would correspond to a SmC mesophase. It is important to mention that on cooling from this SmC phase, the broad signal remains practically unchanged, except for an extra peak appearing in the wide angles region (~4 Å) that could be also attributed to π–π interactions as was previously stated for the T*n-m* compounds. In fact, two more transitions, namely SmC–smectic X (SmX) and SmX–SmX', were observed by DSC between the SmC and the crystallised phase, even though the broad signal in the wide angles region remained unchanged. To determine the exact nature of the SmX and the SmX' mesophases, more studies are still needed. Finally, the layered structure of the mesophases, developed at high temperature, was maintained at room temperature, as was already observed in polypyridinium salts containing pendant mesogenic groups (*26*).

The onset of thermal transitions and enthalpy changes registered upon cooling, as well as the assigned mesophase sequences, are summarised in Table 4.

A number of studies on smectic liquid crystals bearing a pyridinium ring have been published (*15*, *27*) and in most of them the molecular stacking was proposed to be single layered ($d_{001}/L \sim 1$) with upright molecules in a head-to-tail position, even for molecules composed of three parts of different natures, as those presented here. In such reported molecular stacking, positive and negative counter ions face each other creating a double layer of ionic species (*15*). In the present work, we thought that the strong π–π interactions between the long terphenylene cores counterbalance the presumable dominant strong ionic interactions between the ionic species, and assures a full segregation of the three molecular parts in such a way that the head-to-tail arrangement of molecules, usually observed in LC pyridinium salts, is not developed in these molecules. This means that the ionic species, the aromatic cores and the alkyl chains are segregated into three microdomains periodically arranged in space. It is interesting to note that for compounds **P14-8** and **P16-8**, the XRD patterns (Figures 18(a) and 19(a), respectively) showed an additional small sharp Bragg peak from which the calculated layer spacing corresponds to the modelled molecular length, *L*. Differently to the other peaks, this one remains almost in the same position upon cooling. So, it is possible that for a small fraction of the sample, the molecular stacking is single layered with upright molecules in a head-to-tail position, as represented in Figure 20. The competition between two lengths, namely that of the molecule

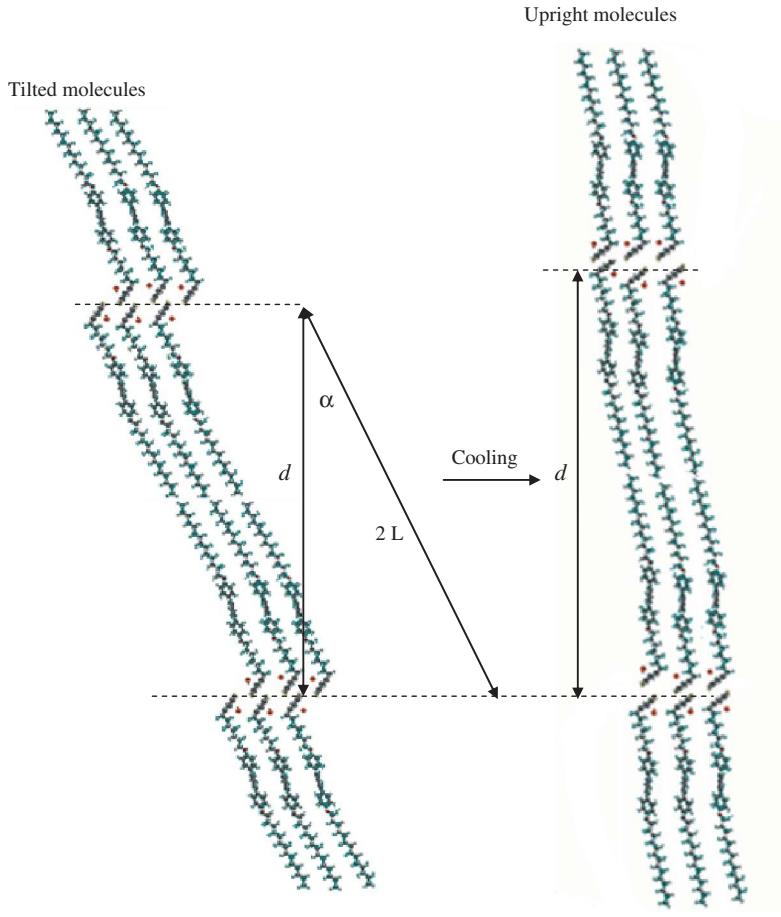

Figure 17. Schematic representation of a double-layered (2*L*) stacking of pyridinium salts.

Table 4. Transition temperatures, enthalpy changes and mesophase sequences for the P*n-m* compounds.

P*n-m*	*T*/°C [ΔH/kJ mol^{-1}]
P14-8	Cr 115.5 [25.58] SmX' 171.5 [2.89] SmX 188.1 [0.83] SmC ~220* I
P14-12	Cr 116.0 [31.89] SmX' 187.3 [3.44] SmX 206.8 [1.51] SmC ~220* I
P16-8	Cr 120.1 [32.55] SmX' 178.4 [4.75] SmX 188.6 [0.86] SmC ~220* I
P16-12	Cr 119.7 [31.83] SmX' 186.3 [3.00] SmX 205.6 [0.95] SmC ~220* I

**Degradation initiates just before the clearing point.*

and that of the pair of antiparallel molecules, has been reported to occur in highly dipolar molecules (*28*). The simultaneous occurrence of two lengths in asymmetric molecules seems to be conditioned to the position of the heads of the molecules with respect to the layers (*29*). In the proposed molecular arrangement models (Figures 17 and 20) for the P*n-m* molecules, the distribution of the ionic species (heads) seems to be satisfactory in both the fully (Figure 17) and the partial (Figure 20) segregated molecular arrangements, as was discussed in a previous work for LC molecules bearing a pyridinium ring, a flexible spacer and a biphenyl core (*15*).

4. Conclusion

Molecules containing a terphenylene group, two flexible chains (terminal and spacer groups) and a pyridinium cycle associated with its bromine counterion were synthesised and their thermotropic LC properties were studied by DSC, POM and XRD. The LC characteristics of pyridinum salts were compared with those of the corresponding chemical intermediate, which also developed an

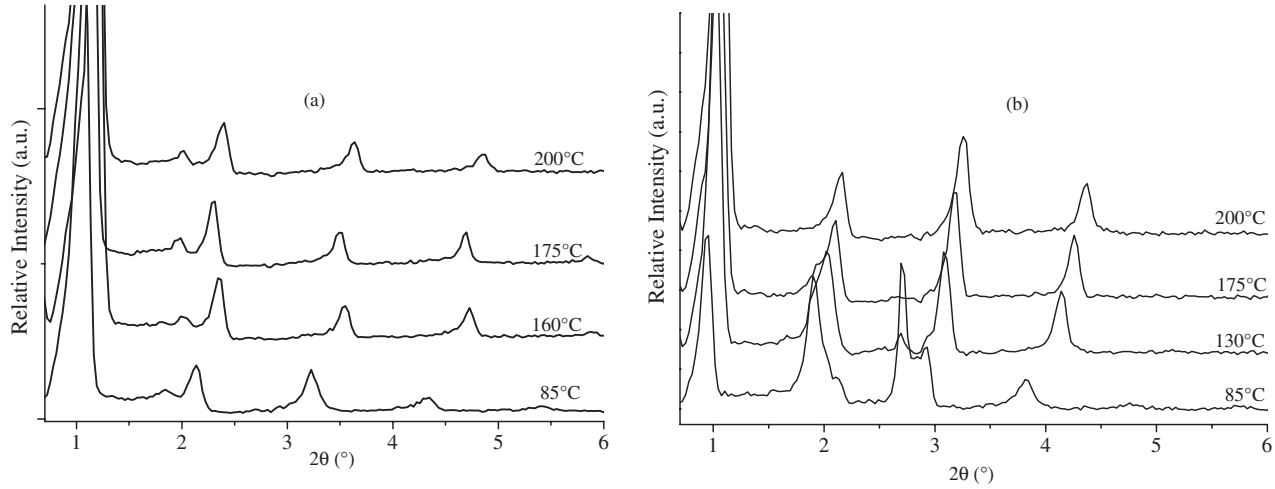

Figure 18. Low angles region of the XRD patterns obtained at different temperatures (upon cooling) for compounds **P14-8** (a) and **P14-12** (b).

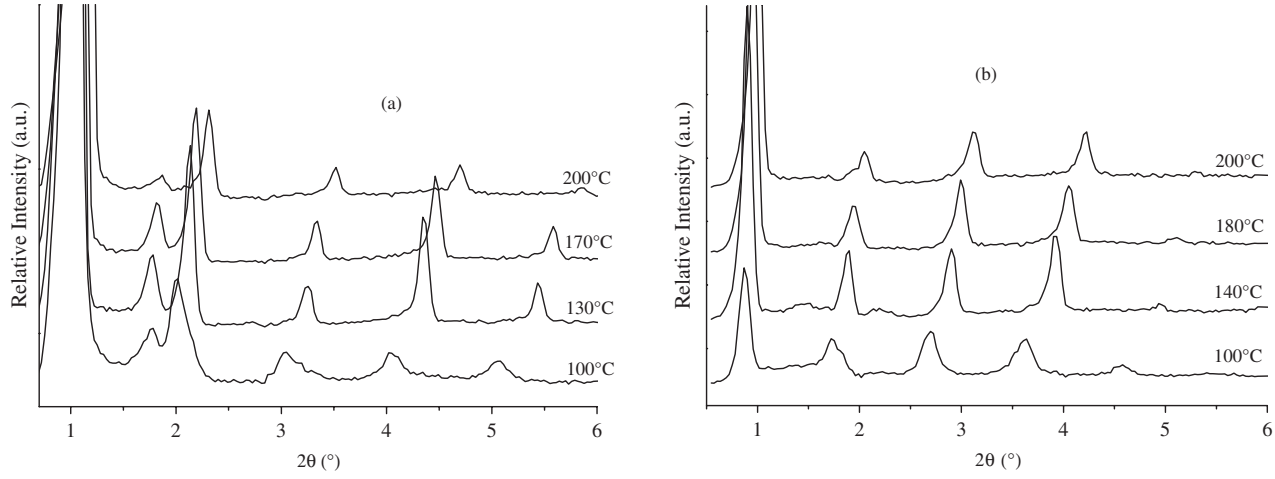

Figure 19. Low angles region of the XRD patterns obtained at different temperatures (upon cooling) for compounds **P16-8** (a) and **P16-12** (b).

interesting mesomorphism. For both compounds tilted smectic-type mesophases were determined, but with important differences in the molecular stacking; smectic phases of intermediates are single layered, whereas those of pyridinium salts are double layered. For both compounds the tilt angle decreases on cooling and in some cases the molecules attain almost an orthogonal position. The proposed molecular arrangement model proposed for the pyridinium salts in the smectic phase is plausible because it is primarily based on both the strong ionic forces and the π–π interactions. Finally, this is an exceptional case where we have found that π–π interactions counterbalance the strong ionic forces leading to a full segregation of molecular parts in smectic structures.

Acknowledgements

We thank the CONACYT of Mexico for supporting this work (project 43741-Y) and for the grant (ref. 202220) given to R. G. Santos-Martell during her MSc studies. We also wish to thank Guadalupe Méndez for her helpful assistance in the thermal characterisation.

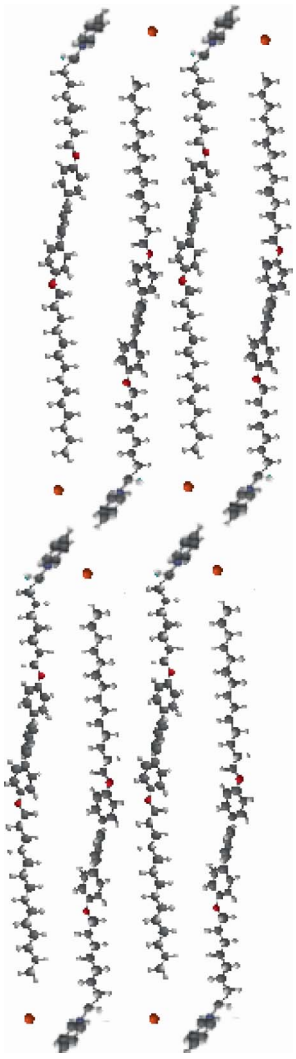

Figure 20. Schematic representation of the stacking of pyridinium salts in a head-to-tail single layered-type smectic phase.

References

(1) O'Neill, M.; Kelly, S.M. *Adv. Mater.* **2003**, *15*, 1135–1146.
(2) Yao Y.-H.; Yang, S.-H.; Hsu, C.-S. *Polymer* **2006**, *47*, 8297–8208.
(3) Lüssem, G.; Festag, R.; Greiner, A.; Schmidt, C.; Unterlechner, C.; Heitz, W.; Wendorff, J.H.; Hopmeier, M.; Feldmann, J. *Adv. Mater*. **1995**, *7*, 923–925.
(4) Sung, H.-H.; Lin, J.H.-C. *Polym. Sci. Part A: Polym. Chem.* **2005**, *43*, 2700–2711.
(5) Misaki, M.; Ueda, Y.; Nagamatsu, S.; Yushida, Y.; Tanigaki, N.; Yase, K. *Macromolecules* **2004**, *37*, 6926–6931.
(6) Aldred, M.P.; Vlachos, P.; Contoret, A.E.A.; Farrar, S.R.; Chung-Tsoi, W.; Mansoor, B.; Woon, K.L.; Hudson, R.; Kelly, S.M.; O'Neill, M. *J. Mater. Chem.* **2005**, *15*, 3208–3213.
(7) Grell, M.; Bradley, D.D.C.; Inbasekaran, M.; Woo, E.P. *Adv. Mater*. **1997**, *9*, 798–802.
(8) Hwang, D.H.; Shim, H.K. *Thin Solid Films* **2002**, *417*, 166–170.
(9) Akagi, K. *Bull. Chem. Soc. Jpn*. **2007**, *80*, 649–661.
(10) Arias, E.; Moggio, I.; Navarro, D.; Romero, J.; Larios, L.; LeMoigne, J.; Guillon, D.; Maillou, T.; González, V.; Geffroy, B. *Rev. Soc. Quím. Mex.* **2002**, *46*, 23–31.
(11) Eastwood, A.J.; Contoret, A.E.A.; Farrar, S.R.; Fowler, S.; Kelly, S.M.; Khan, S.M.; Nicholls, J.E.; O'Neill, M. *Synth. Met.* **2001**, *121*, 1659–1660.
(12) Seoul, C.; Song, W.-J.; Kang, G-W.; Lee, C. *Synth. Met*. **2002**, *130*, 9–16.
(13) Larios-López, L.; Navarro Rodríguez, D.; Arias-Marín, E.M.; Moggio, I.; Reyes-Castañeda, C.V.; Donnio, B.; LeMoigne, J.; Guillon, D. *Liq. Cryst.* **2003**, *30*, 423–433.
(14) Larios-López, L.; Navarro Rodríguez, D.; Donnio, B.; Guillon, D. *Chem. Lett*. **2006**, *35*, 652–653.
(15) Navarro-Rodríguez, D.; Frère, Y.; Gramain, P.; Guillon, D.; Skoulios, A. *Liq. Cryst*. **1991**, *9*, 321–335.
(16) Binnemans, K. *Chem. Rev*. **2005**, *105*, 4148–4204.
(17) Smith, M.B.; March, J. *MARCH'S Advanced Organic Chemistry*, 5th Edn.; John Wiley: New York, 2001.
(18) Miyaura, N.; Suzuki, A. *Chem. Rev.* **1995**, *95*, 2457–2483.
(19) Miyaura, N.; Yanagi, T.; Suzuki, A. *Synth. Commun*. **1981**, *11*, 513–519.
(20) Jing, W.X.; Kraft, A.; Moratti, S.C.; Grüner, J.; Cacialli, F.; Hamer, P.J.; Holmes, A.B.; Friend, R.H., *Synth. Met*. **1994**, *67*, 161–163.
(21) Bravo Grimaldo, E.; Navarro-Rodríguez, D.; Skoulios, A.; Guillon, D. *Liq. Cryst*. **1996**, *20*, 393–398.
(22) Muteau, L.; Caze, C.; Loucheux, C. *Eur. Polym. J.* **1980**, *16*, 1063–1068.
(23) Bunz, U.H.F.; Enkelmann, V.; Kloppenburg, L.; Jones, D.; Shimizu, K.D.; Claridge, J.B.; Loye, H.C.; Lieser, G. *Chem. Mater.* **1999**, *11*, 1416–1424.
(24) Shetty, A.S.; Liu, E.B.; Lachicotte, R.J.; Jenekhe, S.A. *Chem. Mater.* **1999**, *11*, 2292–2295.
(25) Gray, G.W.; Goodby, J.W.G. *Smectic Liquid Crystals Textures and Structures*; Leonard Hill: Glasgow, 1984; pp 45–67.
(26) Navarro-Rodríguez, D.; Guillon, D.; Skoulios, A. *Makromol. Chem*. **1992**, *193*, 3117–3128.
(27) Tabrizian, M.; Soldera, A.; Couturier, M.; Bazuin, G. *Liq. Cryst.* **1995**, *18*, 475–482.
(28) Barois, P.; Coulon, C.; Prost, J. *J. Phys. Lett.* **1981**, *42*, L-107–L-110.
(29) Prost, J. *Adv. Phys.* **1984**, *33*, 170–215.